IEEE Access
Multidisciplinary | Rapid Review | Open Access Journal

Received 13 August 2022, accepted 28 August 2022, date of publication 31 August 2022, date of current version 12 September 2022.

Digital Object Identifier 10.1109/ACCESS.2022.3203052

RESEARCH ARTICLE

Analysis and Robustness Improvement of Finite-Control-Set Model Predictive Current Control for IPMSM With Model Parameter Mismatches

CHAO LI, ZHIHENG LIU, XIANG WU, FENGYOU HE, ZEHAO LV, JIA LI, AND GUOJUN TAN, (Member, IEEE)
School of Electrical Engineering, China University of Mining and Technology, Xuzhou 221008, China
Corresponding author: Xiang Wu (cumtwuxiang@cumt.edu.cn)

This work was supported in part by the National Natural Science Foundational of Jiangsu Province under Award BK20200652, and in part by the National Natural Science Foundational of China under Award 52007190.

ABSTRACT Analysis and robustness improvement of FCS-MPCC for IPMSM with model parameter mismatches are studied in this paper. The prediction error of the current in synchronous rotation coordinate is analyzed and it is divided into two categories according to whether it is related to the selected optimal voltage vector. A robustness improvement method by extracting the information of both kinds of prediction errors in the last sampling period is proposed. The simulation and experimental results demonstrate that the proposed method can effectively improve the ability to resist multiple model parameter mismatches.

INDEX TERMS Model predictive current control, parameter mismatch, interior permanent-magnet synchronous motor.

I. INTRODUCTION

Permanent magnet synchronous motors (PMSMs) including surface-mounted PMSMs (SPMSMs) and interior PMSMs (IPMSMs) have been applied in many industrial fields because of high power density, high efficiency, and excellent performances [1], [2], [3]. Finite-control-set model predictive control (FCS-MPC) [4], [5], [6], [7], [8] has been emerging as one of the promising methods for the control of PMSMs due to its advantages of excellent dynamic performance, nonlinear processing ability, and flexibility to handle multiple constraints and objectives. FCS-MPC obtains the optimal voltage vector according to the predictive model, and thus, its performance highly depends on the accuracy of the model parameters. However, the utilized model parameters in the predicting process of FCS-MPC may not match with the actual ones due to the measurement error and the inevitable change of the inductance, resistance and flux during the operation of PMSMs. Both the steady and dynamic performances of FCS-MPC may be deteriorated with model parameter mismatches [9] and it has been one of the main barriers to its widespread application.

To address the problem, some methods have been studied. The model parameter mismatches can be viewed as one of the disturbances of the system, and the extended state observer [10] has been designed to compensate for model parameter mismatches. In addition, the sliding-model observers (SMO) have also been studied to enhance the robustness [11], [12], [13], [14], [15]. A multistep error tracking based continuous model predictive control with a SMO differentiator is studied in [11] to improve the robustness. A robust predictive speed control for PMSM using integral SMO is proposed in [12]. Robust MPCC based equivalent input disturbance approach for PMSM drive is studied in [13]. The SMO is introduced in the non-cascade predictive control to estimate and compensate the disturbance caused by the uncertain parameters [14]. A continuous integral-type terminal SMO has been studied to deal with the mismatched disturbance [15]. The above disturbances observers are suitable for the continuous model predictive control methods [16], [17],

The associate editor coordinating the review of this manuscript and approving it for publication was Qinfen Lu.

and the methods to combine them with FCS-MPC remain to be solved.

The robustness improvement for FCS-MPC for PMSM has also been studied in recent years. The last prediction errors of a given voltage vector with a weighting factor are added to prediction stage at the presence of inductance uncertainty in [18] to improve the robustness of FCS-MPCC. However, the method in [18] has not considered the parameter mismatches of the stator resistance and the magnetic flux linkage, which make it cannot deal with the cases of multiple parameter mismatches. A cost function in proportional-integral form is introduced in [19] to eliminate the steady-state errors under model parameter mismatches for the finite-control-set model predictive current control (FCS-MPCC) of PMSM. Without quantitative analysis of the prediction errors, the newly designed cost function fails to mitigate the torque ripples and current harmonics caused by parameter mismatches. The methods utilizing current variation or update mechanisms to reconstruct the PMSM model have been studied in [20] and [21] to suppress the disturbances caused by parameter mismatches. An improved FCS-MPCC based on the incremental model for surface-mounted PMSM is studied in [22]. However, the proposed methods in [18], [19], [20], [21], and [22] are all for SPMSMs of which the d-axe and q-axe inductances are viewed as identical. For IPMSMs of which the q-axes inductance is bigger than the d-axe inductance, the prediction error analysis is not fully identical to the methods for SPMSMs, and thus, applying the methods in [18], [19], [20], [21], and [22] to IPMSMs needs further studies. The model free predictive control methods have been studied in [23] and [24], but the measuring noises or errors may lead to instability of the system. An online inductances identification with a recursive algorithm is inherently incorporated into the FCS-MPC of IPMSM to deal with the inductance parameter mismatch [25], however, the parameter mismatches of the resistance and flux have not been considered. The model parameter mismatches for other electrical machines have also been studied [26], [27], [28]. A robust model reference adaptive system estimator incorporating online parameter identification algorithm for parallel predictive torque control of induction motor is studied in [26]. The impact of parameters mismatch on the FCS-MPCC performance of a five-phase induction motor drive is studied in [27]. Influence of covariance-based methods in the performance of predictive controller for five-phase induction motor is studied in [28] to improve the robustness. The models of the motors studied in [26], [27], and [28] are different from IPMSMs, and accordingly, applying the methods in [26], [27], and [28] to IPMSMs needs further studies.

In this paper, analysis and robustness improvement of FCS-MPCC for IPMSM with model parameter mismatches are studied. The prediction errors caused by model parameter mismatches in the two-step prediction considering the time-delay compensation is analyzed. The prediction errors are divided into two categories according to whether it is related to the selected optimal voltage vector. Then, a parameter mismatch compensation method by calculating both kinds of prediction errors according to the error information in last sampling period is proposed. The main contribution of this article is that the prediction errors with model parameter mismatches considering the model of IPMSM is studied and a compensation scheme by calculating the prediction errors with a new and simple method is proposed. The proposed method can deal with multiple parameter mismatches including the stator resistance, magnetic flux linkage, inductances in both d and q axes. The control performances of the proposed method including the steady-state errors of current tracking, current harmonics, and torque ripples can ensure almost the same as the FCS-MPCC without parameter mismatches. The effectiveness of the proposed method is verified by the simulation and experimental results.

II. ANALYSIS OF THE CONVENTIONAL FCS-MPCC FOR IPMSM WITH MODEL PARAMETER MISMATCHES

A. REVIEW OF THE CONVENTIONAL FCS-MPCC CONSIDERING DELAY COMPENSATION

The IPMSM control system based on 2-level voltage source inverter (2L-VSI) is shown in Figure 1 (a). There are 8 switching states for 2L-VSI, which generate 8 different voltage vectors (VVs) (V_0, V_1, $V_2 \ldots V_7$) as shown in Figure 1 (b). The positions of V_0 and V_7 are coincidence and they are defined as zero VVs (ZVVs), and the others are defined as non-zero VVs (NZVVs).

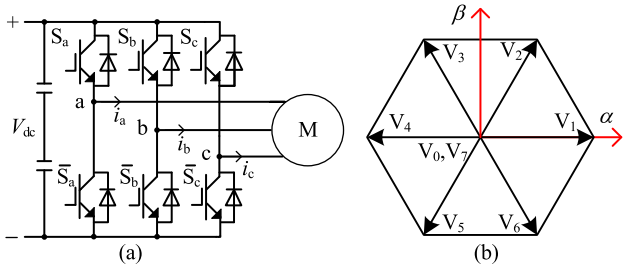

FIGURE 1. PMSM control system based on 2L-VSI. (a) Topology of the 2L-VSI. (b) Voltage vector diagram.

The current predictive equations of IPMSM at the end of kth sampling period are given in (1) and (2)

$$i_{\mathrm{d}}^{\mathrm{p}}(k+1) = \left(1 - \frac{R^{\wedge} T_{\mathrm{s}}}{L_{\mathrm{d}}^{\wedge}}\right) i_{\mathrm{d}}(k) + \omega_{\mathrm{e}} T_{\mathrm{s}} \frac{L_{\mathrm{q}}^{\wedge}}{L_{\mathrm{d}}^{\wedge}} i_{\mathrm{q}}(k) + \frac{T_{\mathrm{s}}}{L_{\mathrm{d}}^{\wedge}} u_{\mathrm{d}}(k) \tag{1}$$

$$i_{\mathrm{q}}^{\mathrm{p}}(k+1) = \left(1 - \frac{R^{\wedge} T_{\mathrm{s}}}{L_{\mathrm{q}}^{\wedge}}\right) i_{\mathrm{q}}(k) - \omega_{\mathrm{e}} T_{\mathrm{s}} \frac{L_{\mathrm{d}}^{\wedge}}{L_{\mathrm{q}}^{\wedge}} i_{\mathrm{d}}(k) - \omega_{\mathrm{e}} T_{\mathrm{s}} \frac{\psi_{\mathrm{f}}^{\wedge}}{L_{\mathrm{q}}^{\wedge}} + \frac{T_{\mathrm{s}}}{L_{\mathrm{q}}^{\wedge}} u_{\mathrm{q}}(k) \tag{2}$$

where R is the stator resistance, ψ_{f} is the magnetic flux linkage, ω_{e} is the electrical angle rotational velocity, u_{d}, i_{d}, and

L_d are the d-axis components of the stator voltage, current, and inductance, u_q, i_q, and L_q are the q-axis components of the stator voltage, current, and inductance, T_s is the sampling period. The motor parameters R, ψ_f, L_d and L_q utilized in the prediction process are defined as $R^\wedge$, $\psi_f^\wedge$, $L_d^\wedge$, and $L_q^\wedge$, respectively.

In order to compensate the time delay in the actuation, two-step prediction is usually used and the corresponding current predictive equations are given in (3) and (4).

$$i_d^p(k+2) = \left(1 - \frac{R^\wedge T_s}{L_d^\wedge}\right) i_d^p(k+1) + \omega_e T_s \frac{L_q^\wedge}{L_d^\wedge} i_q^p(k+1) + \frac{T_s}{L_d^\wedge} u_d(k+1) \tag{3}$$

$$i_q^p(k+2) = \left(1 - \frac{R^\wedge T_s}{L_q^\wedge}\right) i_q^p(k+1) - \omega_e T_s \frac{L_d^\wedge}{L_q^\wedge} i_d^p(k+1) - \omega_e T_s \frac{\psi_f^\wedge}{L_q^\wedge} + \frac{T_s}{L_q^\wedge} u_q(k+1) \tag{4}$$

The cost function is designed as (5) to realize the target of tracking the reference of i_d and i_q. Prediction of the future values of i_d and i_q are calculated for each possible VV and then the VV that minimizes the cost function is selected.

$$g = \left(i_d^* - i_d^p(k+2)\right)^2 + \left(i_q^* - i_q^p(k+2)\right)^2 \tag{5}$$

B. PREDICTION ERROR ANALYSIS CAUSED BY MODEL PARAMETER MISMATCHES

Obviously, prediction equations (1)-(4) contain motor parameters including R, L_d, L_q, and ψ_f. In a real system, motor parameters may vary during operation due to some reasons such as temperature variation, magnetic saturation, and cross-coupling effects. For instance, as the temperature increases, R increases and ψ_f decreases. In addition, the magnetic saturation may result in nonlinear change of L_d and L_q. If the motor parameters utilized in the prediction process deviate from actual values, the current prediction error will be inevitably produced.

The actual currents in d and q axes at the end of kth sampling period are defined as $i_d(k+1)$ and $i_q(k+1)$ and they can be obtained by (1) and (2) if $R^\wedge$, $\psi_f^\wedge$, $L_d^\wedge$, and $L_q^\wedge$ are equal to their actual values. The current prediction errors can be obtained as (6) and (7) with $R^\wedge$, $\psi_f^\wedge$, $L_d^\wedge$, and $L_q^\wedge$ deviating from their actual values

$$\Delta i_d(k+1) = i_d^p(k+1) - i_d(k+1) = C_d + M_d u_d(k) \tag{6}$$

$$\Delta i_q(k+1) = i_q^p(k+1) - i_q(k+1) = C_q + M_q u_q(k) \tag{7}$$

where 'Δ' represents the prediction error, C_d and C_q can be calculated as (8), M_d and M_q can be calculated as (9).

$$\begin{cases} C_d = \left(\frac{R}{L_d} - \frac{R^\wedge}{L_d^\wedge}\right) i_d(k) T_s + \left(\frac{L_q^\wedge}{L_d^\wedge} - \frac{L_q}{L_d}\right) \times \omega_e i_q(k) T_s \\ C_q = \left(\frac{R}{L_q} - \frac{R^\wedge}{L_q^\wedge}\right) i_q(k) T_s + \left(\frac{L_d}{L_q} - \frac{L_d^\wedge}{L_q^\wedge}\right) \times \omega_e i_d(k) T_s + \left(\frac{\psi_f}{L_q} - \frac{\psi_f^\wedge}{L_q^\wedge}\right) \omega_e T_s \end{cases} \tag{8}$$

$$\begin{cases} M_d = \left(\frac{1}{L_d^\wedge} - \frac{1}{L_d}\right) T_s \\ M_q = \left(\frac{1}{L_q^\wedge} - \frac{1}{L_q}\right) T_s \end{cases} \tag{9}$$

As can be seen from (6)-(9), the prediction errors have already appeared in $i_d^p(k+1)$ and $i_q^p(k+1)$. The currents in d and q axes are predicted twice in a whole process to compensate the system delay. The prediction errors appeared in $i_d^p(k+2)$ and $i_q^p(k+2)$ are caused by not only the deviation of the motor parameters but also the prediction errors in $i_d^p(k+1)$ and $i_q^p(k+1)$, which may further increase the prediction errors.

The prediction errors in $i_d^p(k+2)$ and $i_q^p(k+2)$ are

$$\Delta i_d(k+2) = i_d^p(k+2) - i_d(k+2) = C_d^p + M_d u_d(k+1) \tag{10}$$

$$\Delta i_q(k+2) = i_q^p(k+2) - i_q(k+2) = C_q^p + M_q u_q(k+1) \tag{11}$$

where

$$\begin{cases} C_d^p = \left(\frac{R}{L_d} - \frac{R^\wedge}{L_d^\wedge}\right) i_d^p(k+1) T_s + \left(\frac{L_q^\wedge}{L_d^\wedge} - \frac{L_q}{L_d}\right) \omega_e i_q^p(k+1) T_s \\ C_q^p = \left(\frac{R}{L_q} - \frac{R^\wedge}{L_q^\wedge}\right) i_q^p(k+1) T_s + \left(\frac{\psi_f}{L_q} - \frac{\psi_f^\wedge}{L_q^\wedge}\right) \omega_e T_s + \left(\frac{L_d}{L_q} - \frac{L_d^\wedge}{L_q^\wedge}\right) \omega_e i_d^p(k+1) T_s \end{cases} \tag{12}$$

By combining (6)-(12), the prediction errors in $i_d^p(k+2)$ and $i_q^p(k+2)$ can be expressed as

$$\Delta i_d(k+2) = C_d + M_d u_d(k+1) + \gamma_1 \Delta i_d(k+1) + \gamma_2 \Delta i_q(k+1) \tag{13}$$

$$\Delta i_q(k+2) = C_q + M_q u_q(k+1) + \gamma_3 \Delta i_q(k+1) + \gamma_4 \Delta i_d(k+1) \tag{14}$$

where

$$\begin{cases} \gamma_1 = \left(\dfrac{R}{L_\mathrm{d}} - \dfrac{R^\wedge}{L_\mathrm{d}^\wedge}\right) T_\mathrm{s}, \quad \gamma_2 = \left(\dfrac{L_\mathrm{q}^\wedge}{L_\mathrm{d}^\wedge} - \dfrac{L_\mathrm{q}}{L_\mathrm{d}}\right) \omega_\mathrm{e} T_\mathrm{s} \\ \gamma_3 = \left(\dfrac{R}{L_\mathrm{q}} - \dfrac{R^\wedge}{L_\mathrm{q}^\wedge}\right) T_\mathrm{s}, \quad \gamma_4 = \left(\dfrac{L_\mathrm{d}}{L_\mathrm{q}} - \dfrac{L_\mathrm{d}^\wedge}{L_\mathrm{q}^\wedge}\right) \omega_\mathrm{e} T_\mathrm{s} \end{cases} \tag{15}$$

According to (13) and (14), it can be seen that there are two kinds of prediction error. One is from the variation of parameters in the second prediction, the other is from the prediction error produced in the first prediction. Finally, an unexpected voltage vector may be selected in the second prediction according to the cost function defined in (5) due to inaccurate prediction results. The parameter mismatches will have adverse effects on motor operation. Thus, it's necessary to compensate the prediction error to improve the operation performance.

III. ROBUSTNESS IMPROVEMENT OF FCS-MPCC FOR IPMSM WITH MODEL PARAMETER MISMATCH

In accordance with the analysis of part B in section II, two kinds of prediction error should be compensated. If the prediction error in the first prediction has been compensated, i.e., $\Delta i_\mathrm{d}(k+1) = 0$ and $\Delta i_\mathrm{q}(k+1) = 0$, (13) and (14) can be rewritten as

$$\Delta i_\mathrm{d}(k+2) = C_\mathrm{d} + M_\mathrm{d} u_\mathrm{d}(k+1) \tag{16}$$

$$\Delta i_\mathrm{q}(k+2) = C_\mathrm{q} + M_\mathrm{q} u_\mathrm{q}(k+1) \tag{17}$$

The form of (16) and (17) is the same as that of (6) and (7). Once C_d, C_q, M_d and M_q are figured out, $\Delta i_\mathrm{d}(k+1)$ and $\Delta i_\mathrm{q}(k+1)$ can be obtained. Then $\Delta i_\mathrm{d}(k+1)$ and $\Delta i_\mathrm{q}(k+1)$ are compensated in the second prediction. In the end, $\Delta i_\mathrm{d}(k+2)$ and $\Delta i_\mathrm{q}(k+2)$ are fully eliminated by (16) and (17). Accordingly, the key to improve the robustness is to get the values of C_d, C_q, M_d, and M_q. The block diagram of the proposed robustness improvement method is shown in Figure 2.

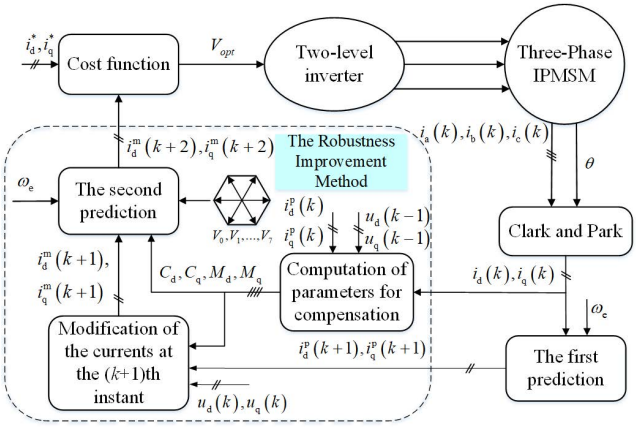

FIGURE 2. Block diagram of the proposed robustness improvement method.

At the kth instant, the current prediction errors in d and q axes are

$$\Delta i_\mathrm{d}(k) = i_\mathrm{d}^\mathrm{p}(k) - i_\mathrm{d}(k) = C_\mathrm{d} + M_\mathrm{d} u_\mathrm{d}(k-1) \tag{18}$$

$$\Delta i_\mathrm{q}(k) = i_\mathrm{q}^\mathrm{p}(k) - i_\mathrm{q}(k) = C_\mathrm{q} + M_\mathrm{q} u_\mathrm{q}(k-1) \tag{19}$$

In (18) and (19), $u_\mathrm{d}(k-1)$ and $u_\mathrm{q}(k-1)$ are known optimal voltage vectors at the $(k-1)$th instant. When the optimal voltage vectors are zero VVs, C_d and C_q are obtained by the difference between the predicted current and actual current as

$$C_\mathrm{d} = i_\mathrm{d}^\mathrm{p}(k) - i_\mathrm{d}(k) \text{ if } u_\mathrm{d}(k-1) = 0 \tag{20}$$

$$C_\mathrm{q} = i_\mathrm{q}^\mathrm{p}(k) - i_\mathrm{q}(k) \text{ if } u_\mathrm{q}(k-1) = 0 \tag{21}$$

Since the sampling period is quite short, it can be considered that the currents in d and q axes remain unchanged between adjacent sampling periods. In the meantime, the motor parameters are also approximately invariant and the rotor speed keeps stable. Hence, if the optimal voltage vectors are non-zero VVs, C_d and C_q can be regarded as equal to the C_d and C_q in the last sampling period, respectively.

When the optimal voltage vectors are non-zero VVs, M_d and M_q can be obtained by (22) and (23) as

$$M_\mathrm{d} = \frac{\Delta i_\mathrm{d}(k) - C_\mathrm{d}}{u_\mathrm{d}(k-1)} \text{ if } u_\mathrm{d}(k-1) \neq 0 \tag{22}$$

$$M_\mathrm{q} = \frac{\Delta i_\mathrm{q}(k) - C_\mathrm{q}}{u_\mathrm{q}(k-1)} \text{ if } u_\mathrm{q}(k-1) \neq 0 \tag{23}$$

When the optimal voltage vectors are zero VVs, M_d and M_q can be viewed as equal to the M_d and M_q in the last sampling period with assuming the motor parameters invariant between adjacent sampling periods.

Since $u_\mathrm{d}(k)$ and $u_\mathrm{q}(k)$ are optimal voltage vectors determined at last sampling period, the current prediction errors at the $(k+1)$th instant can be figured out by (6) and (7). Then the currents after compensation at the $(k+1)$th instant are expressed as

$$\begin{aligned} i_\mathrm{d}^\mathrm{m}(k+1) = {} & \left(1 - \frac{R^\wedge T_\mathrm{s}}{L_\mathrm{d}^\wedge}\right) i_\mathrm{d}(k) + \omega_\mathrm{e} T_\mathrm{s} \frac{L_\mathrm{q}^\wedge}{L_\mathrm{d}^\wedge} i_\mathrm{q}(k) \\ & + \frac{T_\mathrm{s}}{L_\mathrm{d}^\wedge} u_\mathrm{d}(k) - \left(C_\mathrm{d} + M_\mathrm{d} u_\mathrm{d}(k)\right) \end{aligned} \tag{24}$$

$$\begin{aligned} i_\mathrm{q}^\mathrm{m}(k+1) = {} & \left(1 - \frac{R^\wedge T_\mathrm{s}}{L_\mathrm{q}^\wedge}\right) i_\mathrm{q}(k) - \omega_\mathrm{e} T_\mathrm{s} \frac{L_\mathrm{d}^\wedge}{L_\mathrm{q}^\wedge} i_\mathrm{d}(k) \\ & - \omega_\mathrm{e} T_\mathrm{s} \frac{\psi_\mathrm{f}^\wedge}{L_\mathrm{q}^\wedge} + \frac{T_\mathrm{s}}{L_\mathrm{q}^\wedge} u_\mathrm{q}(k) \\ & - \left(C_\mathrm{q} + M_\mathrm{q} u_\mathrm{q}(k)\right) \end{aligned} \tag{25}$$

where 'm' represents the modified value after compensation.

The modified currents are used for the second prediction while the parameter mismatch errors are compensated in the same way. The modified equations in the second prediction are expressed as

$$\begin{aligned} i_\mathrm{d}^\mathrm{m}(k+2) = {} & \left(1 - \frac{R^\wedge T_\mathrm{s}}{L_\mathrm{d}^\wedge}\right) i_\mathrm{d}^\mathrm{m}(k+1) + \omega_\mathrm{e} T_\mathrm{s} \frac{L_\mathrm{q}^\wedge}{L_\mathrm{d}^\wedge} i_\mathrm{q}^\mathrm{m}(k+1) \\ & + \frac{T_\mathrm{s}}{L_\mathrm{d}^\wedge} u_\mathrm{d}(k+1) - \left(C_\mathrm{d} + M_\mathrm{d} u_\mathrm{d}(k+1)\right) \end{aligned} \tag{26}$$

$$i_\mathrm{q}^\mathrm{m}(k+2) = \left(1 - \frac{R^\wedge T_\mathrm{s}}{L_\mathrm{q}^\wedge}\right) i_\mathrm{q}^\mathrm{p}(k+1) - \omega_\mathrm{e} T_\mathrm{s} \frac{L_\mathrm{d}^\wedge}{L_\mathrm{q}^\wedge} i_\mathrm{d}^\mathrm{p}(k+1)$$

$$-\omega_e T_s \frac{\psi_f^{\wedge}}{L_q^{\wedge}} + \frac{T_s}{L_q^{\wedge}} u_q(k+1) - \left(C_q + M_q u_q(k+1)\right) \quad (27)$$

In the end, the modified cost function is given by

$$g^m = \left(i_d^* - i_d^m(k+2)\right)^2 + \left(i_q^* - i_q^m(k+2)\right)^2 \quad (28)$$

The flowchart of the proposed robustness improvement method is shown in Figure 3.

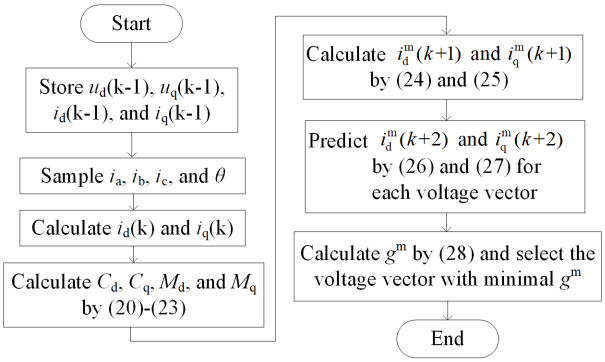

FIGURE 3. Flowchart of the proposed robustness improvement method.

Firstly, the corresponding u_d(k-1) and u_q(k-1) for the selected optimal voltage vector, i_d(k-1), i_q(k-1) are stored to calculate the parameters for compensation. The three-phase currents and the position of the rotor are sampled, and then i_d(k) and i_q(k-1) can be obtained with the Park transformation. The parameters for compensation of the mismatch, i.e., C_d, C_q, M_d, and M_q, are calculated by (20)-(23). Then, the currents after compensation at the $(k+1)$th instant, i.e., $i_d^m(k+1)$, $i_q^m(k+1)$, are calculated according to (24) and (25). The modified currents $i_d^m(k+2)$, $i_q^m(k+2)$ calculated by (26) and (27) are used for the second prediction to compensate the time delay. At last, the modified cost function defined in (28) is evaluated for each voltage vector, and the voltage vector with minimal g_m is selected.

IV. SIMULATION AND ANALYSIS

In order to analyze the effects of the model parameter mismatches on the control performance of FCS-MPCC and verify the effectiveness of the proposed robustness improvement method, simulation is conducted with Matlab software and the parameters of the IPMSM are given in Table 1. The $i_d = 0$ control method is adopted in the simulation. The sample period T_s is set to 60μs and the dc bus voltage is set to 540V.

TABLE 1. Parameters of the IPMSM.

Parameter	Value
Pole pairs	4
Stator resistance	0.1Ω
d-axis inductance	0.95mH
q-axis inductance	2.05mH
Permanent magnet flux linkage	0.225Wb

A. CONTROL PERFORMANCE ANALYSIS FOR FCS-MPCC WITH MODEL PARAMETER MISMATCH

The simulation results with the stator resistance mismatch are shown in Figure 4 and 5, where the reference speed and load torque are 750r/min and 40 N.m, respectively.

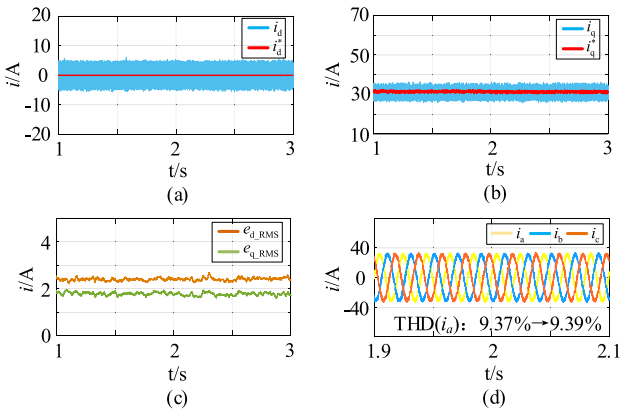

FIGURE 4. Analysis results with the stator resistance mismatch. (a) Curves of i_d (b) Curves of i_q (c) Root mean square values of the error between i_d, i_q and their references (e_{d_RMS}, e_{q_RMS}) (d) Curves of three-phase currents.

In Figure 4, $R^{\wedge}$ is equal to R in the interval of 1-2s and the mismatch happens in the interval of 2-3s where $R^{\wedge}$ is equal to $2R$. According to the curves of i_d, i_q, and the error between i_d, i_q and their references as shown Figure 4 (a)-(c), the stator resistance mismatch has few effects on the control performance of i_d, i_q. The total harmonic distortion (THD) of the phase currents as shown in Figure 4 (d) only increases about 0.02%. In addition, the curves of e_{d_RMS}, e_{q_RMS}, and THD of phase current with different ratios of the stator resistance mismatch are shown in Figure 5, and it is shown that e_{d_RMS}, e_{q_RMS}, and THD of phase current only change slightly with $R^{\wedge}/R$. Accordingly, the effects of the stator resistance mismatch on the steady performance of the conventional FCS-MPCC are not obviously.

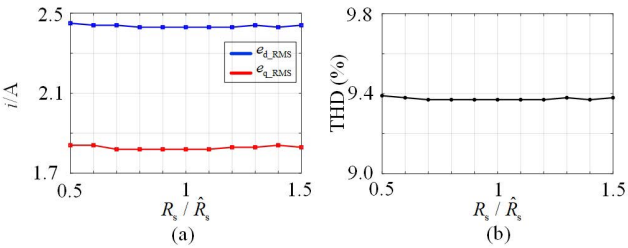

FIGURE 5. Curves of e_{d_RMS}, e_{q_RMS}, and THD of phase current with different ratios of the stator resistance mismatch. (a) e_{d_RMS}, e_{q_RMS} (b) THD of phase current.

The simulation results with the permanent magnet flux linkage mismatch are shown in Figure 6 and 7, where the reference speed and load torque are the same as Figure 3. In Figure 6, $\psi_f^{\wedge}$ is equal to ψ_f in the interval of 1-2s and the mismatch happens in the interval of 2-3s where $\psi_f^{\wedge}$ is equal

to $2\psi_f$. According to the curves of i_d, i_q, and the error between i_d, i_q and their references as shown Figure 6 (a)-(c), the permanent magnet flux linkage mismatch can cause steady errors between i_q and its reference. The total harmonic distortion (THD) of the phase currents as shown in Figure 6 (d) increases about 0.24%.

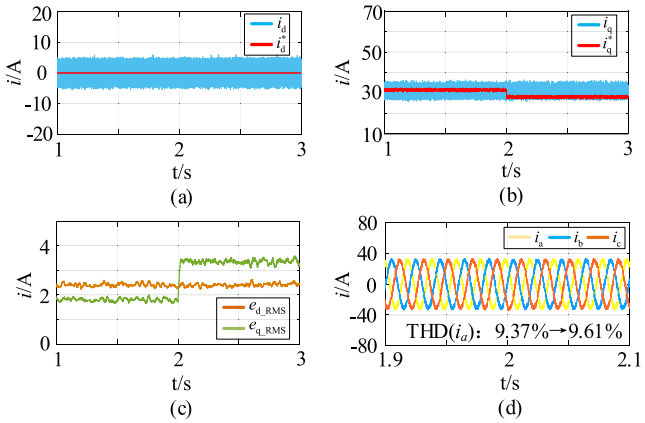

FIGURE 6. Analysis results with the permanent magnet flux linkage mismatch. (a) Curves of i_d (b) Curves of i_q (c) Root mean square values of the error between i_d, i_q and their references (e_{d_RMS}, e_{q_RMS}) (d) Curves of three-phase currents.

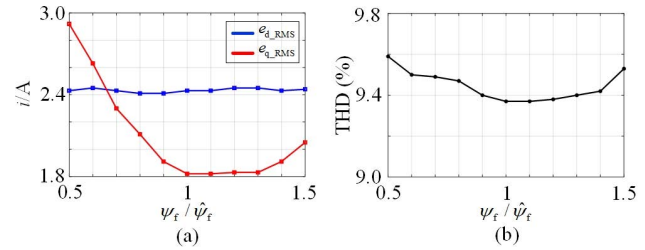

FIGURE 7. Curves of e_{d_RMS}, e_{q_RMS}, and THD of phase current with different ratios of the permanent magnet flux linkage mismatch. (a) e_{d_RMS}, e_{q_RMS} (b) THD of phase current.

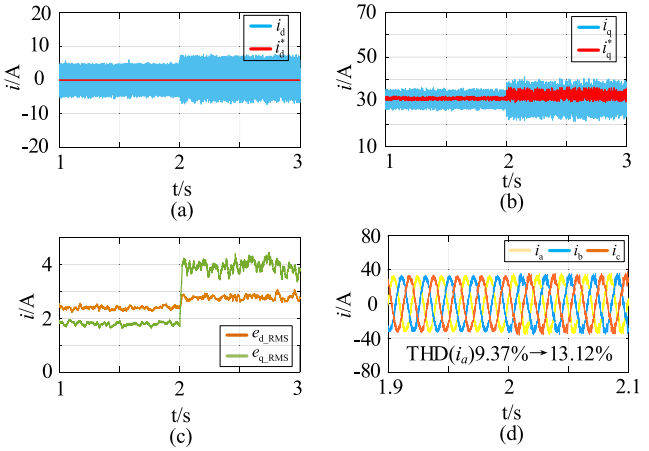

FIGURE 8. Analysis results with L_d mismatch. (a) Curves of i_d (b) Curves of i_q (c) Root mean square values of the error between i_d, i_q and their references (e_{d_RMS}, e_{q_RMS}) (d) Curves of three-phase currents.

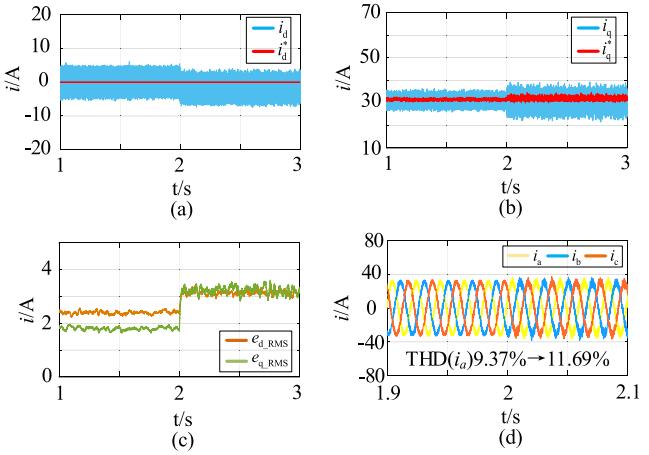

FIGURE 9. Analysis results with L_q mismatch. (a) Curves of i_d (b) Curves of i_q (c) Root mean square values of the error between i_d, i_q and their references (e_{d_RMS}, e_{q_RMS}) (d) Curves of three-phase currents.

In addition, the curves of e_{d_RMS}, e_{q_RMS}, and THD of phase current with different ratios of permanent magnet flux linkage mismatch are shown in Figure 7, and it is shown that e_{q_RMS}, and THD of phase current increase with $\hat{\psi_f}/\psi_f$ deviation from 1.

The simulation results with L_d mismatch are shown in Figure 8, where the reference speed and load torque are the same as Figure 4. In Figure 8, $\hat{L_d}$ is equal to L_d in the interval of 1-2s and the mismatch happens in the interval of 2-3s where $\hat{L_d}$ is equal to $0.5L_d$. According to the curves of i_d, i_q, and the error between i_d, i_q and their references as shown Figure 8 (a)-(c), the L_d mismatch can increase the tracking errors between i_d, i_q and their references. The total harmonic distortion (THD) of the phase currents as shown in Figure 8 (d) increases from 9.37% to 13.12%.

The simulation results with L_q mismatch are shown in Figure 9, where the reference speed and load torque are the same as Figure 4. In Figure 9, $\hat{L_q}$ is equal to L_q in the interval of 1-2s and the mismatch happens in the interval of 2-3s where $\hat{L_q}$ is equal to $1.8L_q$. According to the curves of i_d, i_q, and the error between i_d, i_q and their references as shown Figure 9 (a)-(c), the L_q mismatch can increase the tracking errors between i_d, i_q and their references. The total harmonic distortion (THD) of the phase currents as shown in Figure 9 (d) increases from 9.37% to 11.69%.

Due to the difference between L_d and L_q of IPMSM and the coupling between the model in d and q-axis, the inductance mismatch is much more complex. Figure 10 shows the root mean square values of the error between i_d, i_q and their references (e_{d_RMS}, e_{q_RMS}) with different inductance mismatches. In the case where L_d and L_q change in a small range (no more than $\pm$ 10%), the current errors change very little, indicating that the conventional FCS-MPCC can resist a small range of inductance mismatch. However, both e_{d_RMS} and e_{q_RMS} increase obviously with the mismatch increasing. It can be seen that the inductance mismatch has a greater

impact on the performance of current tracking than the stator resistance and permanent magnet flux linkage mismatches.

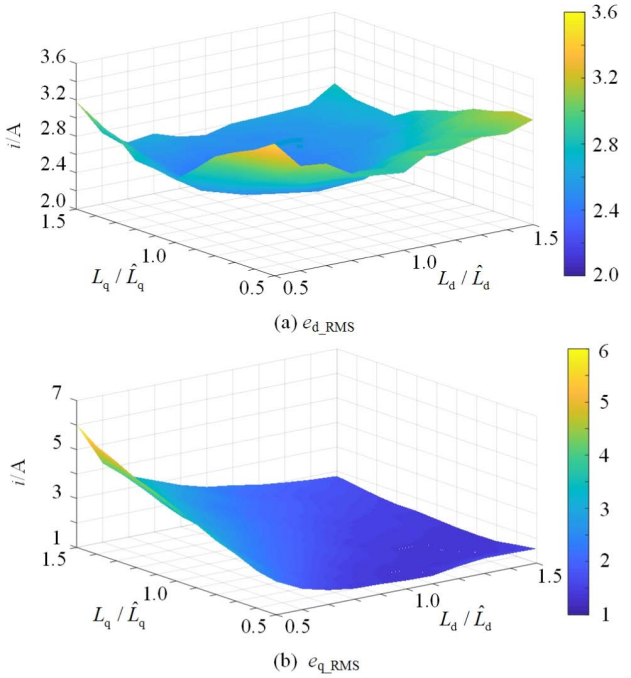

FIGURE 10. Curves of e_{d_RMS} and e_{q_RMS} under different inductance mismatch. (a) e_{d_RMS} (b) e_{q_RMS}.

B. EFFECTIVENESS ANALYSIS OF THE PROPOSED ROBUSTNESS IMPROVEMENT METHOD

To verify the effectiveness of the proposed robustness improvement method, simulation results are given in Figure 11-Figure 15, where the speed reference and load torque are set as 750r/min and 40 N.m respectively. The simulation time is set as 0.8s. The conventional FCS-MPCC is applied before 0.4s, and the proposed robustness improvement method is applied at 0.4s. Multiple parameter mismatches are set in the simulation, i.e., $R^{\wedge}$ is equal to $2R$, $L_d^{\wedge}$ is equal to $0.5L_d$, $L_q^{\wedge}$ is equal to $1.2L_q$, and $\psi_f^{\wedge}$ is equal to $1.25\psi_f$.

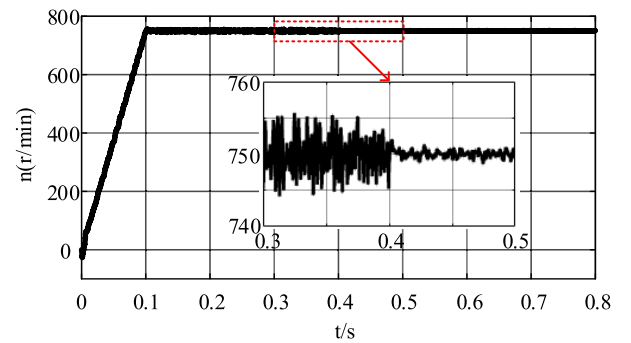

FIGURE 11. Simulation results of the speed.

Simulation results of the speed are shown in Figure 11. According to the enlargement in Figure 11, the biggest value of the speed fluctuation exceeds 10r/min for the conventional FCS-MPCC with multiple parameter mismatches, and it has been reduced to 2.8r/min with the proposed robustness improvement method.

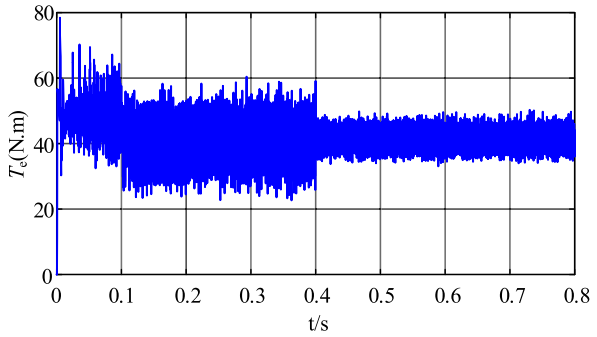

FIGURE 12. Simulation results of the electromagnetic torque.

Simulation results of the electromagnetic torque are shown in Figure 12. The biggest value of the torque fluctuation is about 37.75 N.m for the conventional FCS-MPCC with multiple parameter mismatches, and it has been reduced by about 56.3% with the proposed robustness improvement method.

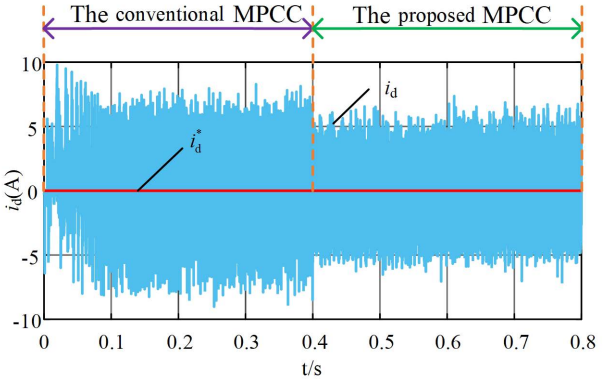

FIGURE 13. Simulation results of i_d.

Simulation results of i_d and i_q are shown in Figure 13 and Figure 14, respectively. By comparing the curves before and after 0.4s, it can be found that the fluctuations of i_d and i_q are large for the conventional FCS-MPCC with multiple parameter mismatches, and they have been successfully reduced with the proposed robustness improvement method…

Simulation results of the phase current (i_a) are shown in Figure 15. The THD of i_a is 18.57% for the conventional FCS-MPCC with multiple parameter mismatches and it has been reduced to 11.37% with the proposed robustness improvement method.

The THD values of i_a with various sample period (T_s) are shown in Figure 16 where the load torque in Figure 16 (a) and (b) is 40 and 80 N.m. The results in Figure 16 indicate that the THD values decrease with the decrease of T_s. Compared with the conventional FCS-MPCC,

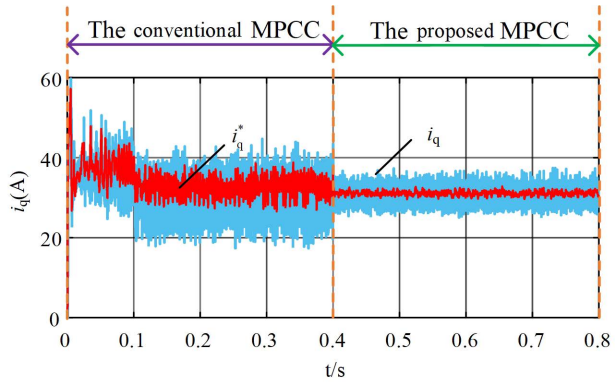

FIGURE 14. Simulation results of i_q.

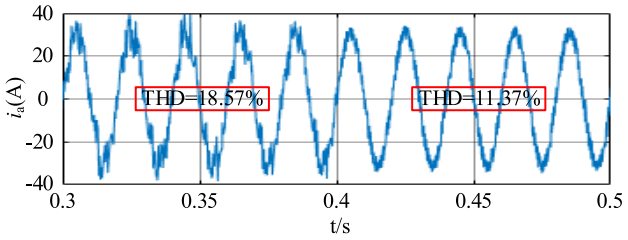

FIGURE 15. Simulation results of i_a.

the current harmonic has been decreased with the proposed FCS-MPCC.

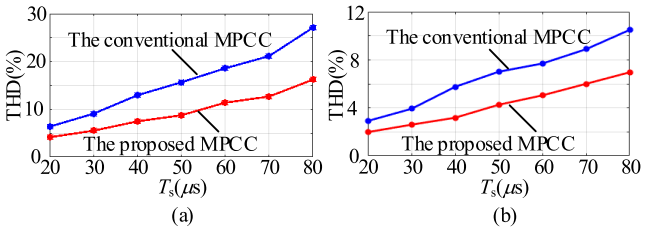

FIGURE 16. THD values of i_a with various sample period. (a) The load torque is 40 N.m. (b) The load torque is 80 N.m.

To analyze the dynamic characteristic of the FCS-MPCC with the proposed robustness improvement method, simulation results with load torque sudden change from 40N.m to 80N.m at 1.0s are shown in Figure 17. The curves of the speed, i_d, and i_q are shown in Figure 17 (a), (b), and (c), respectively. As shown in the enlargement of the speed in Figure 17 (a), the speed can reach its reference in 8ms with the load torque sudden change from 40N.m to 80N.m. The currents can also track their references according to the enlargements of the curves of i_d and i_q.

Accordingly, the above simulation results indicate the FCS-MPCC with the proposed robustness improvement method can realize satisfied steady-state and dynamic performances with model parameter mismatches.

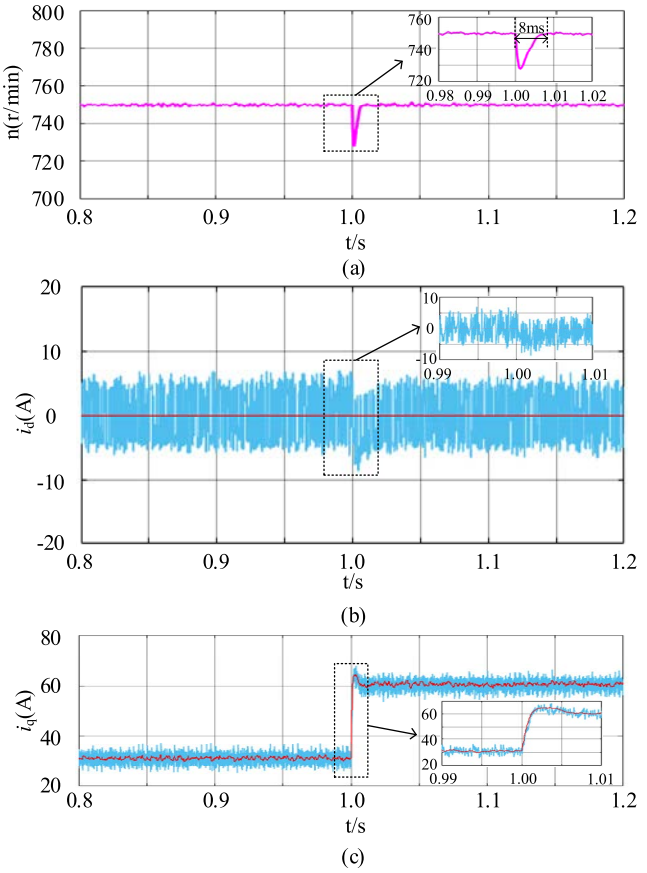

FIGURE 17. Simulation results with load torque sudden change. (a) Speed (b) i_d (c) i_q.

C. COMPARATIVE ANALYSIS

Comparative analysis is given in this part to illustrate the advantages of the proposed method. Comparative results of i_q, i_d, i_a, and the root-mean-square values of the electromagnetic torque ripples are given in Figure 18-21, where the results of the conventional FCS-MPCC without parameter mismatches, the conventional FCS-MPCC with parameter mismatches, the robust FCS-MPCC proposed in [19] and the proposed FCS-MPCC are shown in Figure 18-21 (a), (b), (c), and (d), respectively. Two cases of parameter mismatches are simulated, i.e., in the process of ① as shown in Figure 18-21, $R^\wedge$ is equal to $2R$, $L_d^\wedge$ is equal to $0.5L_d$, $L_q^\wedge$ is equal to $1.2L_q$, and $\psi_f^\wedge$ is equal to $1.25\psi_f$, while, in the process of ②, $R^\wedge$ is equal to $0.5R$, $L_d^\wedge$ is equal to $2L_d$, $L_q^\wedge$ is equal to $0.5L_q$, and $\psi_f^\wedge$ is equal to $0.4\psi_f$. In Figure 18-21, the speed reference and load torque are set as 750r/min and 80 N.m respectively.

By observing Figure 18, the fluctuation of i_q for the conventional FCS-MPCC in the parameter mismatches process of ① increases obviously compared with the conventional FCS-MPCC without parameter mismatches. In addition, there is a steady-state error of i_q in the parameter mismatches process of ② for the conventional FCS-MPCC. As shown in Figure 18 (c), the steady-state error of i_q in the parameter mismatches process of ② can be mitigated with the robust FCS-MPCC proposed in [19] where a newly designed cost

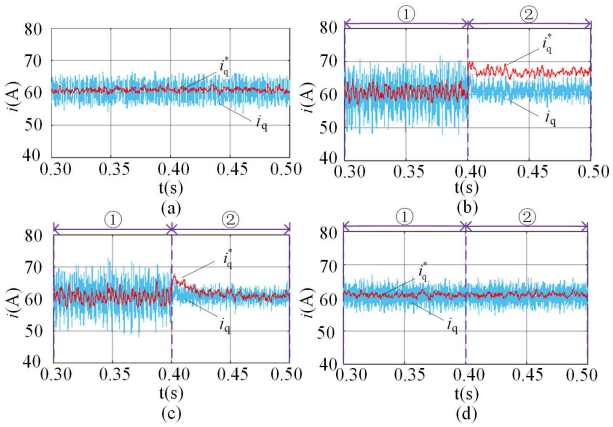

FIGURE 18. Comparative results of i_q. (a) The conventional FCS-MPCC without parameter mismatches (b) The conventional FCS-MPCC with parameter mismatches (c) The FCS-MPCC proposed in [19] (d) The proposed FCS-MPCC.

function in proportional-integral form is adopted. However, the fluctuation of i_q as shown in Figure 18 (c) is still high. With the proposed FCS-MPCC, both the steady-state error and the fluctuation have been decreased. The curves shown in Figure 18 (d) for the proposed FCS-MPCC are almost the same as Figure 18 (a) for the conventional FCS-MPCC without parameter mismatches.

By observing Figure 19, the fluctuation of i_d for the conventional FCS-MPCC in the parameter mismatches process of ① increases obviously compared with the conventional FCS-MPCC without parameter mismatches.

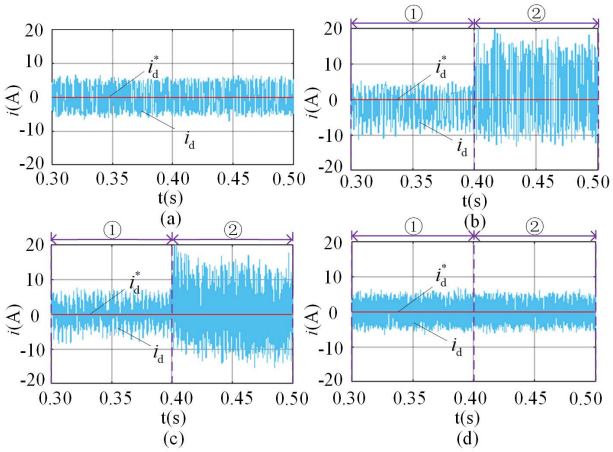

FIGURE 19. Comparative results of i_d. (a) The conventional FCS-MPCC without parameter mismatches (b) The conventional FCS-MPCC with parameter mismatches (c) The FCS-MPCC proposed in [19] (d) The proposed FCS-MPCC.

In addition, there is a steady-state error of i_d in the parameter mismatches process of ② for the conventional FCS-MPCC. As shown in Figure 19 (c), the steady-state error of i_d in the parameter mismatches process of ② can be mitigated with the robust FCS-MPCC proposed in [19]. However, the fluctuation of i_d as shown in Figure 19 (c) is still high. With the proposed FCS-MPCC, both the steady-state error and the fluctuation of i_d have been decreased. The curves shown in Figure 19 (d) for the proposed FCS-MPCC are almost the same as Figure 19 (a) for the conventional FCS-MPCC without parameter mismatches.

As shown in Figure 20 (a), the THD value of i_a for the conventional MPCC without parameter mismatches is 4.87%, and it increases to 8.54% and 8.94% in the parameter mismatches process of ① and ②, respectively. The harmonic contents in the phase current increase substantially with the conventional MPCC in the process of parameter mismatches. As shown in Figure 20 (c), the THD values of i_a for the robust MPCC proposed in [19] are 7.95% and 8.86% in the parameter mismatches process of ① and ②, respectively. The THD values in the phase current decrease to 4.93% and 4.97% with the proposed method, which are similar as the conventional MPCC without parameter mismatches.

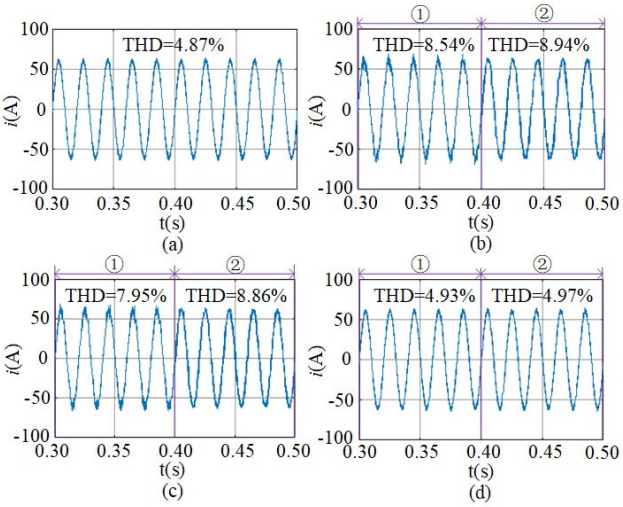

FIGURE 20. Comparative results of i_a. (a) The conventional FCS-MPCC without parameter mismatches (b) The conventional FCS-MPCC with parameter mismatches (c) The FCS-MPCC proposed in [19] (d) The proposed FCS-MPCC.

As shown in Figure 21, the fluctuation of T_e for the conventional FCS-MPCC in the parameter mismatches process increases obviously compared with the conventional FCS-MPCC without parameter mismatches. The root-mean-square value of the electromagnetic torque ripples ($\hat{T}_{e\_RMS}$) for the conventional FCS-MPCC without parameter mismatches is 2.51 N.m, and it increases to 5.52 and 3.01 N.m in the parameter mismatches process of ① and ②, respectively. The ripples in the electromagnetic torque increase substantially with the conventional MPCC in the process of parameter mismatches. As shown in Figure 21 (c), $\hat{T}_{e\_RMS}$ has been reduced slightly with the method in [19]. With the proposed method, $\hat{T}_{e\_RMS}$ has been reduced to 2.52 and 2.53N.m, which are similar as the FCS-MPCC without parameter mismatches.

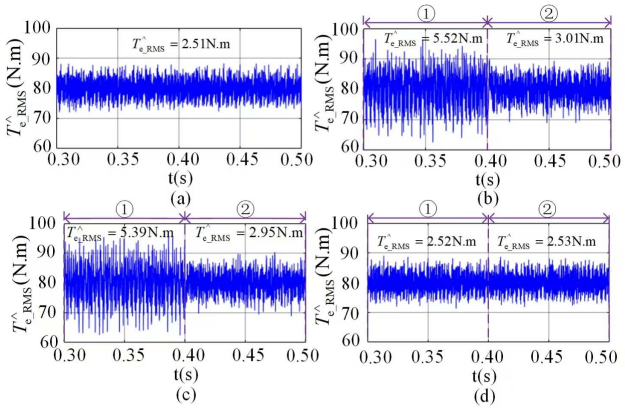

FIGURE 21. Comparative results of T_e. (a) The conventional FCS-MPCC without parameter mismatches (b) The conventional FCS-MPCC with parameter mismatches (c) The FCS-MPCC proposed in [19] (d) The proposed FCS-MPCC.

Comparative results of $T^{\wedge}_{e\_RMS}$ with various load torque are shown in Figure 22. In the two cases of the parameter mismatches, both the torque ripples can be greatly reduced with the proposed method. For the parameter mismatches process of ① , the torque ripples of the proposed method, as shown in Figure 22(a) have been reduced by more than 54.4% compared with the conventional FCS-MPCC. For the parameter mismatches process of ②, the torque ripples of the proposed method, as shown in Figure 22(b) have been reduced by more than 16.3% compared with the conventional FCS-MPCC. The newly designed cost function in proportional-integral form in [19] is helpful to decrease the steady-state error of i_d and i_q. According to the comparative results shown in Figure 18-22, the proposed method can realize better performances than the FCS-MPCC proposed in [19] in the aspects of current harmonics and torque ripples.

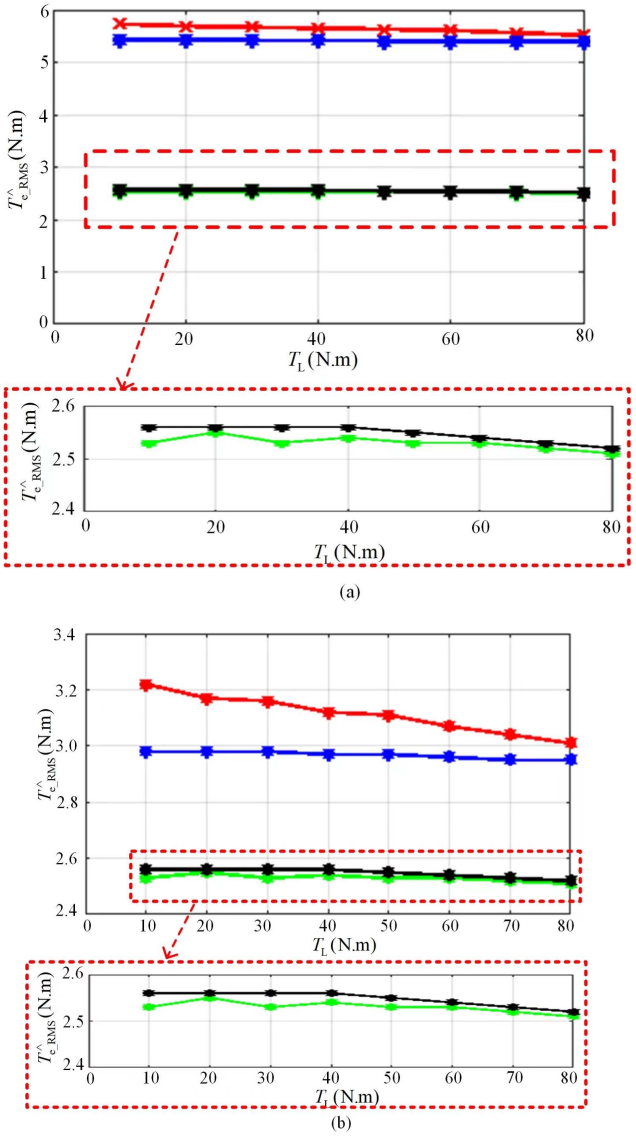

FIGURE 22. Comparative results of $T^{\wedge}_{e\_RMS}$ with various load torque. (a) $R^{\wedge}$ is equal to $2R$, $L^{\wedge}_d$ is equal to $0.5L_d$, $L^{\wedge}_q$ is equal to $1.2L_q$, and $\psi^{\wedge}_f$ is equal to $1.25\psi_f$ (b) $R^{\wedge}$ is equal to $0.5R$, $L^{\wedge}_d$ is equal to $2L_d$, $L^{\wedge}_q$ is equal to $0.5L_q$, and $\psi^{\wedge}_f$ is equal to $0.4\psi_f$.

V. EXPERIMENTAL VERIFICATION

The proposed MPCC is implemented on a PMSM drive platform of which the photos are shown in Figure 23. The experimental platform includes a TMSF28377D control board, 2L-VSI, power supply, PC, the tested IPMSM (Motor 1) and an extra IPMSM to offer the load torque (Motor 2). Motor 2 is controlled by another inverter and it can work in both speed and torque control mode. The proposed FCS-MPCC is implemented on a 4 pole-pairs IPMSM drive platform based on a 2L-VSI of which the dc bus voltage is about 540V. The current probes are adopted to measure the phase current and the curves of id, iq, and the speed are measured with a digital-to-analog chip on the control board. The stator resistance (R_0), d-axis inductance (L_{d0}), q-axis inductance (L_{q0}), permanent magnet flux linkage (ψ_{f0}) of the IPMSM which are obtained by off-line identification are 0.1Ω, 0.95mH, 2.05mH, and 0.225Wb, respectively. For the FCS-MPCC, the sampling period (T_s) is set as 60μs. The reference of i_q is obtained by a proportional-integral-controller based speed control loop and the reference of i_d is set as 0. In the experiment, the reference of the speed is set as 750 r/min and the load torque is about 50N.m.

The experimental results for both the conventional and proposed FCS-MPCC with parameter mismatches are given in Figure 24-26, where the parameters adopted in the prediction satisfy $R^{\wedge} = 3R_0$, $L^{\wedge}_d = 0.4L_{d0}$, $L^{\wedge}_q = 4L_{q0}$, and $\psi^{\wedge}_f = 2\psi_{f0}$.

Curves of i_d and i_q of the conventional and proposed FCS-MPCC are shown in Figure 24 and Figure 25, respectively. It can be seen that both i_d and i_q of the conventional FCS-MPCC can not accurately track the reference current under this case. The steady-state error of i_d and i_q caused by parameter mismatches for the conventional FCS-MPCC is about 26.8A and 27.5A, respectively. Fortunately, with the

proposed robustness improvement method, the steady-state error of i_d and i_q have been reduced to 0.67A and 1.65A, respectively. It's even worse that there are large distortions on the currents for the conventional method, i.e., the root mean square value of the tracking error of i_d and i_q is about 31.38A and 32.76A, respectively. Fortunately, with the proposed robustness improvement method, the root mean square value of the tracking error of i_d and i_q has been reduced to 9.28A and 5.65A, respectively. For the conventional FCS-MPCC with parameter mismatches, the poor current tracking will deteriorate system performances. Conversely, the proposed FCS-MPCC achieves fairly good current tracking performances.

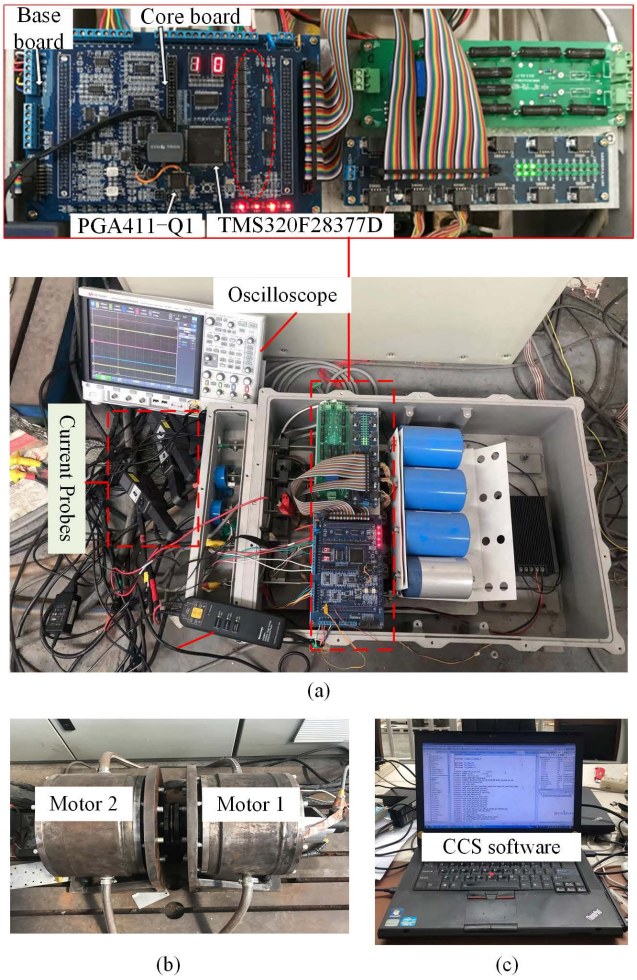

FIGURE 23. Photos of the experimental platform. (a) 2L-VSI (b) The tested and load motors (c) PC with CCS software.

The current of phase 'a' of the IPMSM (i_a) is also measured in the steady state, which is shown in Figure 26. In the conventional FCS-MPCC, the waveform is greatly distorted resulting from parameter mismatches. The THD of i_a as shown in Figure 26 (a) is 25.30% and there are a large amount of low-order harmonics. By the implementation of the proposed robustness improvement method, the current quality can be

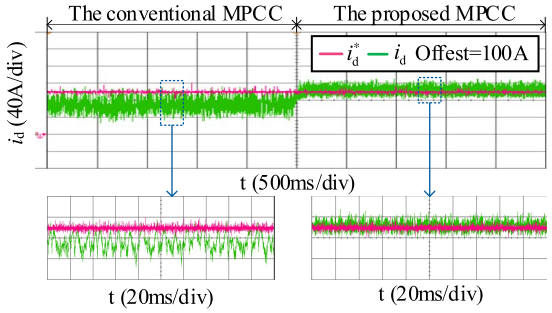

FIGURE 24. Curves of i_d of the conventional and proposed FCS-MPCC.

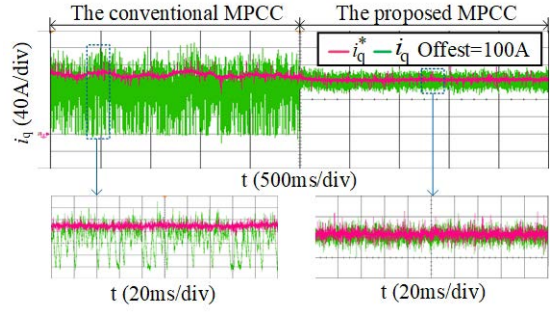

FIGURE 25. Curves of i_q of the conventional and proposed FCS-MPCC.

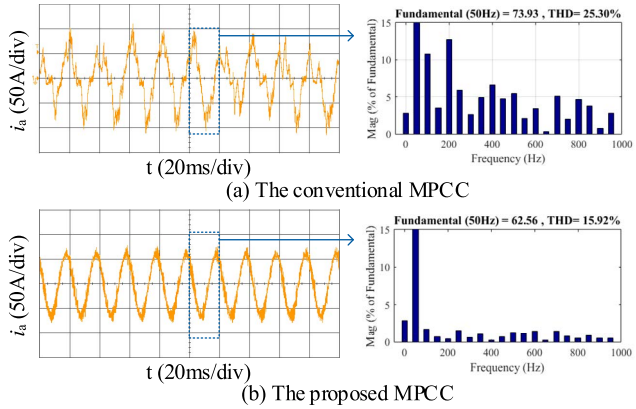

FIGURE 26. Curves of i_a of the conventional and proposed FCS-MPCC.

effectively promoted as shown in Figure 26(b) and the THD has been reduced to 15.92%.

Accordingly, the above analysis indicates that the proposed robustness improvement method is effective and it can achieve satisfactory performance in the case where multiple parameters of IPMSM are mismatched. Compared with the conventional FCS-MPCC for IPMSM, the proposed method increases some computational complexity. The implementation time of the proposed increases about 1.7 μs, which is only 2.83% of the sampling period. Accordingly, the increased computational complexity has little impact with the adopted TMSF28377D control board.

The current transient response results with the proposed method is shown in Figure 27. The speed keeps 750 r/min

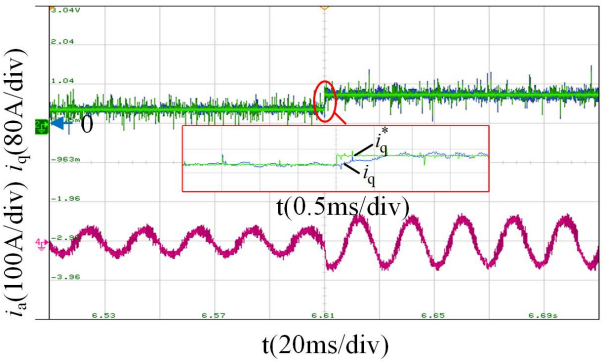

FIGURE 27. Current transient response results with the proposed FCS-MPCC.

through the speed controller of the load motor and the reference of i_q for the tested IPMSM changes suddenly from 30A to 60A. According to the enlargement in Figure 27, i_q can track the step change within 0.65ms, which indicate the excellent dynamic performance of the proposed method.

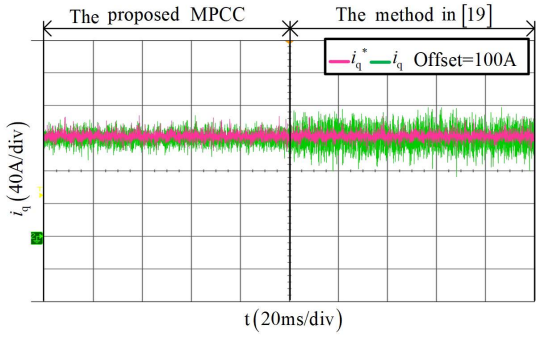

FIGURE 28. Comparative results of i_q between the proposed method and the method proposed in [19].

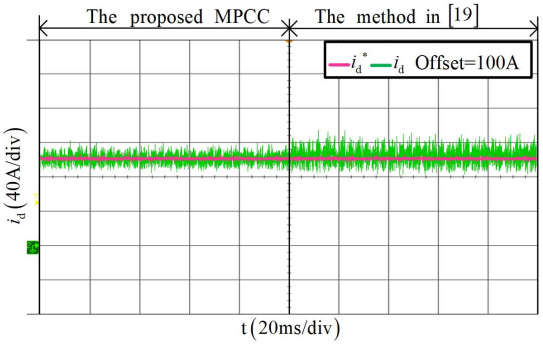

FIGURE 29. Comparative results of i_d between the proposed method and the method proposed in [19].

Comparative analysis between the proposed method and the robust FCS-MPCC proposed in [19] is experimentally studied. Comparative results of i_q and i_d are shown in Figure 28 and 29, respectively. By comparing Figure 25 with Figure 28, the steady-state error of i_q can be mitigated with both the proposed method and the method in [19]. The root-mean square values of the ripples of i_q with the proposed method and the method in [19] are 5.65 and 25.64A. By comparing Figure 24 with Figure 29, the steady-state error of i_d can be mitigated with both the proposed method and the method in [19]. The root-mean square values of the ripples of i_d with the proposed method and the method in [19] are 9.28 and 19.32A. Accordingly, the proposed method can realize better performances in the aspect of current tracking compared with the previously studied method in [19].

VI. CONCLUSION

In this paper, the prediction error caused by model parameter mismatches in the two-step prediction considering the time-delay compensation is analyzed and a robustness improvement method is proposed to depress the model parameter sensitivity. The conclusion is given as follows:

1) The prediction errors with parameter mismatches of the stator resistance, magnetic flux linkage, inductances in both d and q axes are studied. The mismatches of stator resistance and magnetic flux linkage mainly cause the steady-state error of the current tracking, while the mismatches of inductances cause both the steady-state error and the increase of the current ripples.

2) The parameter mismatch compensation method by calculating the prediction errors which have been divided into two kinds can mitigate the steady-state error of the current tracking and reduce the current harmonics caused by parameter mismatches.

3) The simulation and experimental results indicate that the proposed method can deal with multiple parameter mismatches and the control performances of the proposed method including the steady-state errors of current tracking, current harmonics, and torque ripples can ensure almost the same as the FCS-MPCC without parameter mismatches. The torque ripples of the proposed method can be reduced by more than 54.4% and 16.3% compared with the conventional FCS-MPCC in the parameter mismatches process of ① and ②, respectively.

REFERENCES

[1] A. Nasr, C. Gu, X. Wang, G. Buticchi, S. Bozhko, and C. Gerada, "Torque-performance improvement for direct torque-controlled PMSM drives based on duty-ratio regulation," *IEEE Trans. Power Electron.*, vol. 37, no. 1, pp. 749–760, Jan. 2022.

[2] L. Nguyen and T. C. Pham, "Optimal tracking control for PMSM with partially unknown dynamics, saturation voltages, torque, and voltage disturbances," *IEEE Trans. Ind. Electron.*, vol. 69, no. 4, pp. 3481–3491, Apr. 2022.

[3] X. Wu, Z. Lv, Z. Ling, X. Zhang, and G. Tan, "An improved pulse voltage injection based initial rotor position estimation method for PMSM," *IEEE Access*, vol. 9, pp. 121906–121915, 2021.

[4] Z. Zhang, Z. Li, M. P. Kazmierkowski, J. Rodríguez, and R. Kennel, "Robust predictive control of three-level NPC back-to-back power converter PMSG wind turbine systems with revised predictions," *IEEE Trans. Power Electron.*, vol. 33, no. 11, pp. 9588–9598, Nov. 2018.

[5] F. Wang, K. Zuo, P. Tao, and J. Rodriguez, "High performance model predictive control for PMSM by using stator current mathematical model self-regulation technique," *IEEE Trans. Power Electron.*, vol. 35, no. 12, pp. 13652–13662, Dec. 2020.

[6] A. Bakeer, H. S. Salama, and I. Vokony, "Integration of PV system with SMES based on model predictive control for utility grid reliability improvement," *Protection Control Modern Power Syst.*, vol. 6, no. 1, pp. 191–203, Dec. 2021.

[7] F. Yu, K. Li, Z. Zhu, and X. Liu, "An over-modulated model predictive current control for permanent magnet synchronous motors," *IEEE Access*, vol. 10, pp. 40391–40401, 2022.

[8] O. Arpacik and M. M. Ankarali, "An efficient implementation of online model predictive control with field weakening operation in surface mounted PMSM," *IEEE Access*, vol. 9, pp. 167605–167614, 2021.

[9] H. A. Young, A. Perez, and J. Rodriguez, "Analysis of finite-control-set model predictive current control with model parameter mismatch in a three-phase inverter," *IEEE Trans. Ind. Electron.*, vol. 63, no. 5, pp. 3100–3107, May 2016.

[10] Y. Zhang, J. Jin, and L. Huang, "Model-free predictive current control of PMSM drives based on extended state observer using ultralocal model," *IEEE Trans. Ind. Electron.*, vol. 68, no. 2, pp. 993–1003, Feb. 2021.

[11] F. Wang, L. He, and J. Rodriguez, "FPGA-based continuous control set model predictive current control for PMSM system using multistep error tracking technique," *IEEE Trans. Power Electron.*, vol. 35, no. 12, pp. 13455–13464, Dec. 2020.

[12] F. Wang and L. He, "FPGA-based predictive speed control for PMSM system using integral sliding-mode disturbance observer," *IEEE Trans. Ind. Electron.*, vol. 68, no. 2, pp. 972–981, Feb. 2021.

[13] X. Liu and Q. Zhang, "Robust current predictive control-based equivalent input disturbance approach for PMSM drive," *Electronics*, vol. 8, no. 9, p. 1034, Sep. 2019.

[14] Y. Wang and X. Liu, "Model predictive position control of permanent magnet synchronous motor servo system with sliding mode observer," *Asian J. Control*, vol. 19, pp. 1–19, Apr. 2022.

[15] X. Liu and H. Yu, "Continuous adaptive integral-type sliding mode control based on disturbance observer for PMSM drives," *Nonlinear Dyn.*, vol. 104, no. 2, pp. 1429–1441, Mar. 2021.

[16] X. Jiang, Y. Yang, M. Fan, A. Ji, Y. Xiao, X. Zhang, W. Zhang, C. Garcia, S. Vazquez, and J. Rodriguez, "An improved implicit model predictive current control with continuous control set for PMSM drives," *IEEE Trans. Transport. Electrific.*, vol. 8, no. 2, pp. 2444–2455, Jun. 2022.

[17] X. Zhang, G. H. B. Foo, T. Jiao, T. Ngo, and C. H. T. Lee, "A simplified deadbeat based predictive torque control for three-level simplified neutral point clamped inverter fed IPMSM drives using SVM," *IEEE Trans. Energy Convers.*, vol. 34, no. 4, pp. 1906–1916, Dec. 2019.

[18] M. Siami, D. A. Khaburi, A. Abbaszadeh, and J. Rodríguez, "Robustness improvement of predictive current control using prediction error correction for permanent-magnet synchronous machines," *IEEE Trans. Ind. Electron.*, vol. 63, no. 6, pp. 3458–3466, Jun. 2016.

[19] X. Liu, L. Zhou, J. Wang, X. Gao, Z. Li, and Z. Zhang, "Robust predictive current control of permanent-magnet synchronous motors with newly designed cost function," *IEEE Trans. Power Electron.*, vol. 35, no. 10, pp. 10778–10788, Oct. 2020.

[20] X. Yuan, S. Zhang, C. Zhang, A. Galassini, G. Buticchi, and M. Degano, "Improved model predictive current control for SPMSM drives using current update mechanism," *IEEE Trans. Ind. Electron.*, vol. 68, no. 3, pp. 1938–1948, Mar. 2021.

[21] X. Yuan, S. Zhang, and C. Zhang, "Nonparametric predictive current control for PMSM," *IEEE Trans. Power Electron.*, vol. 35, no. 9, pp. 9332–9341, Sep. 2020.

[22] X. Zhang, L. Zhang, and Y. Zhang, "Model predictive current control for PMSM drives with parameter robustness improvement," *IEEE Trans. Power Electron.*, vol. 34, no. 2, pp. 1645–1657, Feb. 2019.

[23] F. Tinazzi, P. G. Carlet, S. Bolognani, and M. Zigliotto, "Motor parameter-free predictive current control of synchronous motors by recursive least-square self-commissioning model," *IEEE Trans. Ind. Electron.*, vol. 67, no. 11, pp. 9093–9100, Nov. 2020.

[24] C. Ma, H. Li, X. Yao, Z. Zhang, and F. De Belie, "An improved model-free predictive current control with advanced current gradient updating mechanism," *IEEE Trans. Ind. Electron.*, vol. 68, no. 12, pp. 11968–11979, Dec. 2021, doi: 10.1109/TIE.2020.3044809.

[25] Z. Chen, J. Qiu, and M. Jin, "Adaptive finite-control-set model predictive current control for IPMSM drives with inductance variation," *IET Elect. Power Appl.*, vol. 11, no. 5, pp. 874–884, Oct. 2017.

[26] H. Xie, F. Wang, Y. He, J. Rodriguez, and R. Kennel, "Encoderless parallel predictive torque control for induction machine using a robust model reference adaptive system," *IEEE Trans. Energy Convers.*, vol. 37, no. 1, pp. 232–242, Mar. 2022.

[27] C. Martín, M. Bermúdez, F. Barrero, M. R. Arahal, X. Kestelyn, and M. J. Durán, "Sensitivity of predictive controllers to parameter variation in five-phase induction motor drives," *Control Eng. Pract.*, vol. 68, pp. 23–31, Nov. 2017.

[28] J. Rodas, C. Martin, M. R. Arahal, F. Barrero, and R. Gregor, "Influence of covariance-based ALS methods in the performance of predictive controllers with rotor current estimation," *IEEE Trans. Ind. Electron.*, vol. 64, no. 4, pp. 2602–2607, Apr. 2017.

CHAO LI was born in Shandong, China, in 1996. He received the B.S. degree in electrical engineering and automation from the China University of Mining and Technology, Xuzhou, China, in 2018, where he is currently pursuing the M.S. degree in power electronics and electrical drives with the School of Electrical and Power Engineering.

His research interests include power electronics, modern control theory, and motor.

ZHIHENG LIU was born in Shandong, China, in 1999. He received the B.S. degree in electrical engineering from the Qilu University of Technology, Jinan, China, in 2021. He is currently pursuing the M.S. degree in power electronics and electrical drives with the School of Electrical and Power Engineering, China University of Mining and Technology, Xuzhou, China.

His current research interests include permanent magnet synchronous motor drives and model predictive control.

XIANG WU was born in Jiangsu, China, in 1990. He received the B.S. and Ph.D. degrees in electrical engineering and automation from the University of Mining and Technology, Xuzhou, China, in 2013 and 2019, respectively.

He is currently a Lecturer of power electronics and electrical drives with the School of Electrical and Power Engineering, China University of Mining and Technology. His research interests include power electronics, modern control theory, battery management systems, and motor drives.

FENGYOU HE was born in Hebei, China, in 1963.

He was a Senior Visiting Scholar at the University of Duisburg-Essen, Germany. Since 2003, he has been a Professor with the China University of Mining and Technology, Xuzhou, China. He has long been committed to power electronics and power transmission control technology, network automation control technology, and information management technology and its application. He has presided over and participated in many projects, such as national "863" projects, the National Natural Science Foundation of China, the National Technological Innovation Project, the Natural Science Foundation of Jiangsu Province, and the School-Enterprise Horizontal Cooperation Projects. His research interests include the transmission system of large mine hoist and belt conveyors in China.

ZEHAO LV was born in Zhejiang, China, in 1997. He received the B.S. degree in electrical engineering from Fuzhou University, Fuzhou, China, in 2019. He is currently pursuing the M.S. degree in power electronics and electrical drives with the School of Electrical and Power Engineering, China University of Mining and Technology, Xuzhou, China.

His current research interests include permanent magnet synchronous motor drives and model predictive control.

JIA LI was born in Jiangsu, China, in 1998. She received the B.S. degree from Huaiyin Normal University, Huaian, China, in 2021. She is currently pursuing the M.S. degree in power electronics and electrical drives with the School of Electrical and Power Engineering, China University of Mining and Technology, Xuzhou, China.

Her research interests include power electronics, modern control theory and motor, permanent magnet synchronous motor drives, and model predictive control.

GUOJUN TAN (Member, IEEE) was born in Zunyi, Guizhou, China, in 1962. He received the Ph.D. degree in motor driver and it's automation from the China University of Mining and Technology, Xuzhou, China, in 1992.

Since 2000, he has been a Professor with the School of Information and Electrical Engineering, China University of Mining and Technology. Since 2003, he has been the Chief Professor of the National Key Discipline on power electronics and motor driver in this school. His main research interests include electrical drive, intelligent algorithm, and system optimization.